PAPER

Check for updates

Luminescent cyclometalated alkynylplatinum(II) complexes with 1,3-di(pyrimidin-2-yl)benzene ligands: synthesis, electrochemistry, photophysics and computational studies†

Mariia Hruzd, [ID] [a] Nicolas le Poul, [ID] [b] Marie Cordier,[a] Samia Kahlal,[a] Jean-Yves Saillard, [ID] [a] Sylvain Achelle, [ID] *[a] Sébastien Gauthier [ID] *[a] and Françoise Robin-le Guen*[a]

In this article, we report on a series of cyclometalated chloro- and alkynyl-platinum(II) complexes bearing various tridentate N^C^N-cyclometalated ligands derived from 1,3-bis(pyrimidin-2-yl)benzene. The X-ray crystal structures of two alkynyl-platinum(II) complexes were determined and other structures were DFT-calculated. Electrochemical and DFT-computational studies suggest a ligand-centred reduction on the R^1-substituted N^C^N ligand, whereas oxidation likely occurs either on the Pt-phenylacetylide moiety and/or the cyclometalated ligand. In CH_2Cl_2 solution at room temperature, the complexes show phosphorescent emissions ranging from green to orange, depending on the R^1 and R^2 substituents on the ligands. In KBr solid state matrix, excluding complexes bearing a trifluoromethyl substituted ligand, all compounds exhibit red emission. The presence of an alkynyl ancillary ligand has limited influence on absorption and emission spectra except in the case of the complex with the strongly electron-donating diphenylamino R^2 substituent on the alkynyl ligand, for which a significant red-shift was observed. The alkynyl Pt(II) complex with OMe groups as both R^1 and R^2 substituents shows the best emission quantum yield (0.81 in CH_2Cl_2 solution) in this series. The full series of DFT calculated band gaps correlated generally well with the electrochemical and absorption data and reasonably model the impact of the substituents on the electronics of these complexes.

Introduction

Luminescent organometallic complexes have attracted considerable interest over the past few decades in the area of functional molecular materials, notably for their applications in photocatalysis,[1–4] luminescence sensing and cellular imaging,[5–7] as well as in organic light-emitting diode (OLED) devices.[8–11] The main advantage of employing organometallic complexes as emitters for the fabrication of highly efficient phosphorescent OLEDs is their capacity to access triplet states *via* intersystem crossing (ISC) from the singlet excited state

[a]Univ. Rennes, CNRS, ISCR (Institut des Sciences Chimiques de Rennes) – UMR 6226, F-35000 Rennes, France. E-mail: sylvain.achelle@univ-rennes1.fr, sebastien.gauthier@univ-rennes1.fr, francoise.le-guen@univ-rennes1.fr

[b]Laboratoire de Chimie, Électrochimie Moléculaires et Chimie Analytique, UMR CNRS 6521, Université de Bretagne Occidentale, UFR Sciences et Techniques, 6 avenue Victor Le Gorgeu – CS 93837, F-29238 Brest Cedex 3, France

†Electronic supplementary information (ESI) available. CCDC 2126978 and 2126979. For ESI and crystallographic data in CIF or other electronic format see DOI: 10.1039/d1dt04237h

through strong spin–orbit coupling mediated by the heavy metal in the complexes.[12–17]

Phosphorescent transition metal compounds, such as iridium(III),[18] platinum(II),[19,20] ruthenium(II),[21] osmium(II)[22] and gold(III) complexes[23] have proven to be an outstanding class of emitter materials for making OLEDs because of their high luminescence quantum yields. The photophysical properties of luminescent metal complexes could be directly modulated by an appropriate variation of ligands and metal ions.[24,25] A large number of highly phosphorescent materials are coordination compounds based on cyclometalated complexes.[23,26,27] The combination of rigidity of the molecule, strong metal–chelate bonding, substituent effect on ligands and design of the ligand skeleton may contribute to improving the luminescence quantum efficiency and tuning the color of the emission of the resulting cyclometalated complexes.[28]

Among them, cyclometalated platinum(II) complexes represent an important class of phosphorescent materials due to their interesting coordination geometry and rich photochemical and photophysical properties in solution and in solid state.[29–31] Notably, their four-coordinated square-planar

structure can accommodate bidentate, tridentate, or tetradentate chelating ligands[32–37] and additional ancillary ligands,[38–40] which offers considerable options for engineering targeted highly phosphorescent materials. It has been shown that electronic excited states and their relative energies can be improved *via* modifications the coordinated ligands around the platinum ion.[41–43] Furthermore, the planar geometry of the platinum complexes facilitates interesting specific self-assembly behaviors and luminescence properties of the complexes by intermolecular π···π stacking or axial Pt···Pt interactions.[44–48]

Recently a series of tridentate cyclometalated [Pt(N^C^N)Cl] complexes with an electron-deficient pyrimidine-contained N^C^N ligands have been synthesized by Jin and co-workers, and as reported, the replacement of one pyridine with a pyrimidine ring in N^C^N platinum(II) complexes affect the intermolecular interactions and the luminescence properties of the complexes.[49] However, no supplementary studies in this series of complexes have been carried out to enhance the photophysical properties by substitution of the chloride by ancillary acetylide ligands. In fact, Williams and co-workers have reported that the substitution of the chloride ligand of cyclometalated [PtLCl] complex (L = 5-methyl-1,3-di(2-pyridyl) benzene) by 3,5-difluorophenyl-acetylide induces higher photoluminescence quantum yields than the corresponding chloride complex (Φ_{PL} = 0.77 *vs.* 0.68).[50] In addition, complementary studies have demonstrated that the Pt(II) acetylide complexes are interesting because the excited and luminescence properties of the complexes can be optimized by variation of the substituent in the σ-alkynyl auxiliary.[51–54]

In this context, this study aims to develop high-efficiency emitters based on cyclometalated chloro- and alkynyl-platinum complexes bearing a 1,3-bis(pyrimidin-2-yl)benzene derivative ligands. The effect of substitution of the monodentate ancillary ligand (chloride or various substituted phenylacetylides) and the introduction of different groups to the central phenyl ring of the N^C^N ligands on the complexes 1–14 have been investi-

gated experimentally and theoretically (Fig. 1). The results show that the incorporation of electro-donating or electro-withdrawing groups on both the tridentate and σ-alkynyl ligands in these complexes can result in tuning and, in some case, improving their photophysical properties in solution and in solid state.

Results and discussion

Synthesis and characterization

The synthesis of the complexes requires the cyclometalating tridentate N^C^N ligands 18–20 whose preparation was accomplished in a two-step synthesis as previously reported (synthetic scheme is provided in ESI, Scheme S1†).[49] In a first step, the arylboronate ester derivatives 15–17 were produced by Pd-catalyzed Miyaura borylation cross-coupling reaction of 1,3-dibromobenzene derivatives with bis(pinacolato)diboron in the presence of PdCl$_2$(dppf) and a weak base KOAc in DMF at 90 °C in moderate yield. In the second step, the arylboronate ester derivatives 15–17 were converted into the corresponding ligands 18–20 under Pd-catalyzed Suzuki–Miyaura cross-coupling reaction in presence of the 2-chloropyrimidine, Pd(PPh$_3$)$_4$ and K$_2$CO$_3$ (aq) under reflux of toluene in moderate to good yields. The N^C^N cyclometalated chloro-platinum(II) complexes 1 and 2 are known compounds and were prepared as previously reported method.[49,55] The chloro-platinum(II) precursor complexes 3 was obtained using a similar procedure in a good yield, after a 2-day reaction between the corresponding ligand 20 and potassium tetrachloroplatinate (K$_2$PtCl$_4$) in a refluxed solution of glacial acetic acid (Scheme 1). Finally, N^C^N cyclometalated alkynyl-platinum(II) complexes 4–14 were prepared under conventional cross-coupling condition by reaction of chloro-platinum(II) precursors 1–3 with the corresponding organic alkynes in the presence of sodium methoxide and MeOH/CH$_2$Cl$_2$ (4 : 1 v/v) at 40 °C.[56] Due to his low solubility, chloro-platinum complex 3 has only been characterized by
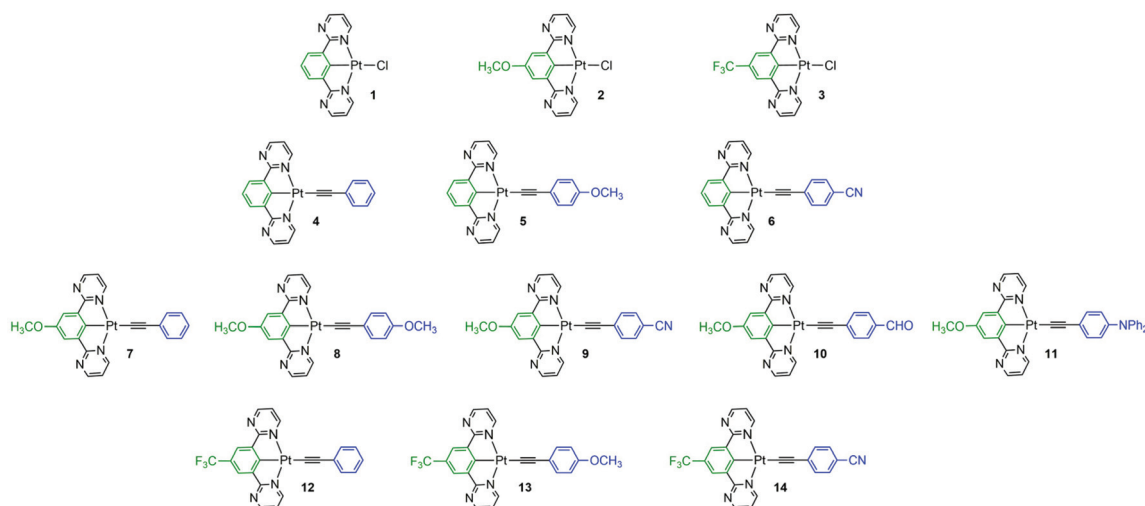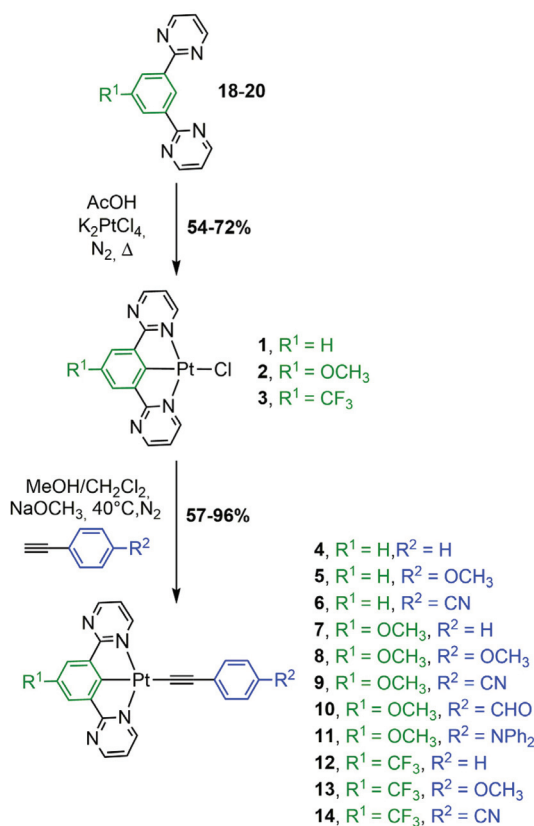

Fig. 1 Chemical structures of the cyclometalated platinum-based complexes 1–14 investigated in this work.

HRMS. Alkynyl-platinum complexes **4–14** were analyzed by ^{1}H NMR, IR and HRMS. The characterization data were found to be in complete agreement with the proposed structures.

X-ray crystal structures

Single crystals of alkynyl-platinum complexes **7** and **8** were obtained by slow evaporation of CH$_2$Cl$_2$ solution of the complex at room temperature, and their molecular structures were determined by X-ray crystallography analysis as shown in Fig. 2(A) and Fig. 3(A). The crystal data and structure refinement details are provided in the ESI (Tables S2 and S3†), and selected bond lengths and bond angles are listed in Table 1. As generally observed for cyclometalated N^C^N and C^N^N

Scheme 1 Synthesis of N^C^N cyclometalated chloro-platinum(II) complexes **1–3** and alkynyl-platinum(II) complexes **4–14**.

Table 1 Selected X-ray bond distances (Å) and angles (°) of complexes **7** and **8**. Corresponding DFT-computed values are given into brackets

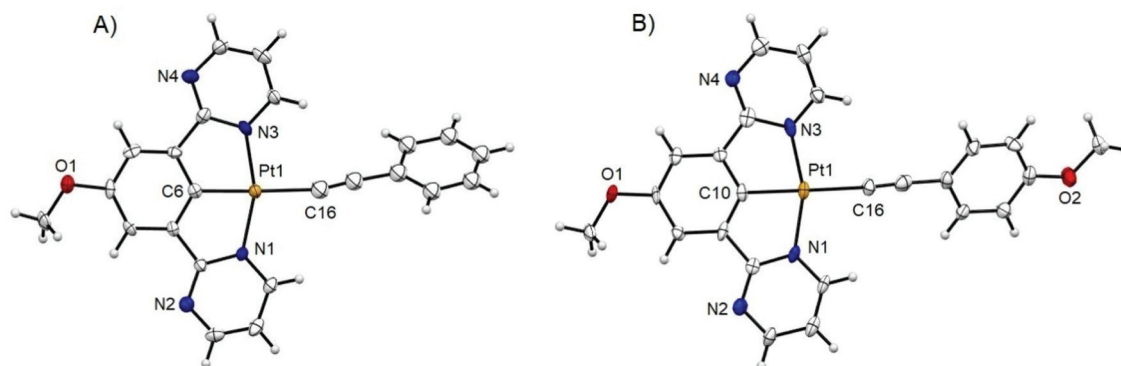| Complex 7		Complex 8	
Pt1–C6	1.951(8) [1.940]	Pt–C10	1.949(8) [1.939]
Pt1–N3	2.029(7) [2.039]	Pt1–N3	2.036(7) [2.039]
Pt1–N1	2.030(6) [2.039]	Pt1–N1	2.040(7) [2.039]
Pt1–C16	2.125(8) [2.046]	Pt1–C16	2.092(8) [2.047]
C6–Pt1–N3	80.30(3) [79.50]	C10–Pt1–N3	79.70(3) [79.49]
C6–Pt1–N1	79.00(3) [79.39]	C10–Pt1–N1	79.30(3) [79.38]
N3–Pt1–N1	159.30(2) [158.89]	N3–Pt1–N1	158.90(3) [158.87]
C6–Pt1–C16	176.80(4) [179.91]	C10–Pt1–C16	175.30(3) [179.81]
N3–Pt1–C16	98.10(3) [100.53]	N3–Pt1–C16	99.40(3) [100.50]
N1–Pt1–C16	102.50(3) [100.59]	N1–Pt1–C16	101.60(3) [100.63]
Pt⋯Pt	3.300	Pt⋯Pt	4.683
π–π	~3.30	π–π	3.401

Fig. 2 ORTEP drawings of complex **7** (A) and **8** (B). Thermal ellipsoids are set at 50% probability level.
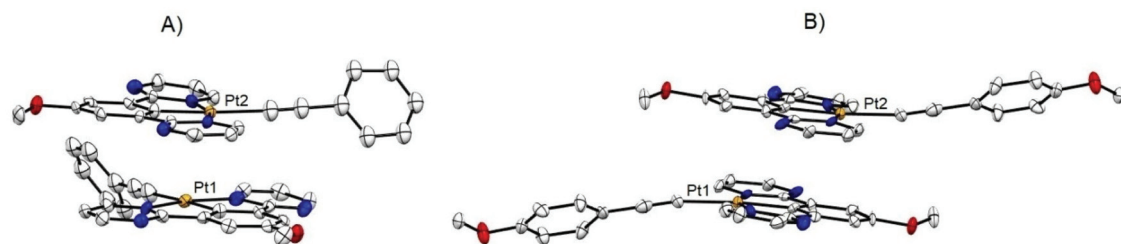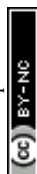
Fig. 3 ORTEP drawings of the crystal packing structure in dimeric form: (A) complex **7** showing the staggered configuration, (B) complex **8** showing the head-to-tail configuration. Thermal ellipsoids are set at 50% probability level. Hydrogen atoms have been omitted for clarity.

platinum(II) complexes, the Pt(II) ion center of complexes **7** and **8** adopts a distorted square-planar geometry defined by a tridentate cyclometalated ligand **19** and one alkynyl fragment.[51,54,57,58] The N–Pt–C and N–Pt–N angles (C6–Pt1–N3 80.30°, C6–Pt1–N1 79.00° and N3–Pt1–N1 159.30° for complex **7**, and C10–Pt1–N3 79.70°, C10–Pt1–N3 79.30°, N3–Pt1–N1 158.90° for complex **8**) are found to deviate from the idealized value of 180° and 90°, respectively. The Pt–N bond distances in the two complexes **7** and **8** are 2.029–2.040 Å, comparable to those in the reported analogue [Pt(N^C^N)Cl] complexes. The bond lengths Pt–C16 for complex **7** and **8** are 2.125 and 2.092 Å, respectively. Complex **7** and **8** have a longer Pt–C(N^C^N) bond lengths (Pt1–C6 1.951 Å for **7** and Pt1–C10 1.949 Å for **8**), which can be attributed to the higher *trans* influence of the alkynyl ligand than that of the chloride ligand.

Notably intermolecular interactions and conformations have been observed in these crystal lattices of complexes **7** and **8** (Fig. 3(A and B). The crystal packing of complex **7** show a staggered stacking arrangement between pairs of complex molecules (Fig. 3(A)). Intermolecular π···π interaction was found in the crystal packing, and the distance between the vertical plane-to-plane separation ($d_{\pi-\pi}$) of two adjacent molecules is ~3.30 Å. The closest Pt–Pt distance (d_{Pt-Pt}) in the crystal of **7** is only 3.300 Å, which is indicative of strong metal–metal interactions. The crystal packing of complex **8** show a head-to-tail stacking arrangement between pairs of complex molecules (Fig. 3(B)). Intermolecular π···π interaction have been detected in the crystal packing, and the distance between the vertical plane-to-plane separation ($d_{\pi-\pi}$) of two adjacent molecules is ~3.40 Å. There is no Pt···Pt interaction for **8**, the shortest Pt–Pt distance (4.683 Å) of **8** is much longer than **7**. The divergence can be attributed to the difference in structural arrangement created by the addition of a methoxy group on the phenyl ring.

Electrochemical properties

Cyclic voltammograms of the chloro-platinum complexes **1–3** display an irreversible and broad peak at $E_{pa}(1)$ at *ca.* 0.6–0.8 V *vs.* Fc⁺/Fc upon scanning in the positive direction (Fig. 4(A)). The value of $E_{pa}(1)$ varies with R¹, as evidenced by the most positive value obtained with complex **3** (see Table 2). On the cathodic part, a single reduction peak is detected at $E_{pc}(3)$ (Table 3 and Fig. 4(A)). This peak is irreversible at $v = 0.1$ V s⁻¹, but displays more reversibility when the scan rate is increased (inset, Fig. 4(A)). The value of $E_{pc}(3)$ is R¹-dependent, consistent with a reduction process on the phenyl ligand. Noteworthy, this redox behavior is slightly different from that found for pyridine-based N^C^N Pt complexes,[55] although experimental conditions were not fully the same (DMF *vs.* CH₂Cl₂). Indeed, replacement of the two pyridine rings by two pyrimidine units induces of loss of reversibility of the reduction process. Moreover, both oxidation and reduction processes are shifted towards more positive potential values by approximatively 200 mV, as shown by the comparative data for H- and OMe-phenyl-based Pt complexes. Such a result is consistent with the stronger electron-deficient properties of the pyrimidine *vs.* pyridine moieties.
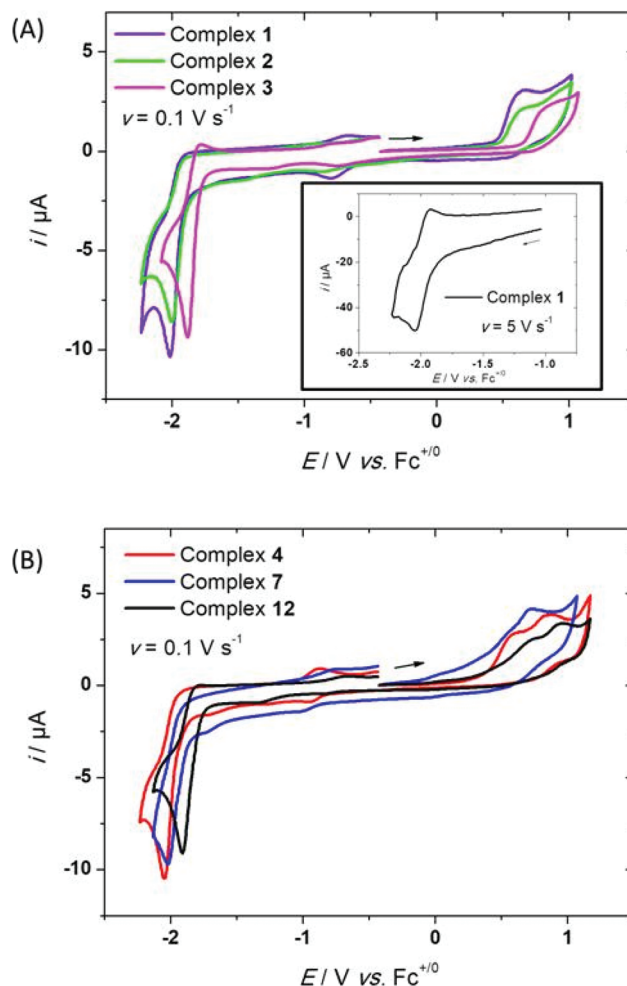

Fig. 4 Cyclic voltametry (CV) at a Pt working electrode (*E*/V *vs.* Fc⁺/Fc) of (A) chloro-platinum complexes **1**, **2** and **3** (*v* = 0.1 V s⁻¹) and (B) alkynyl-platinum complexes **4**, **7** and **12** in CH₂Cl₂/NBu₄PF₆ 0.1 M under inert atmosphere. *C* = 0.5 mM. Inset (A): CV of complex **1** at *v* = 5 V s⁻¹.

As shown in Fig. 4(B) and Table 2, alkynyl-complexes **4–14** display similar behavior to **1–3**. On one hand, the value of $E_{pc}(3)$ varies with the electronic properties of R¹ as for complexes **1–3**, in agreement with a reduction process on the Pt-bound phenyl ligand, the values being close to those found for the chloride complexes. On the other hand, the irreversible oxidation process at $E_{pa}(1)$ does not sensibly change with R² for this series, as previously found for analogous Pt complexes.[31]

For instance, alkynyl-complexes **4**, **7** and **12** (R² = H) display similar values to their chloro-platinum analogues (complexes **1**, **2** and **3** respectively). Within a single R¹ series such as for complexes **7–11**, the oxidation potential seems independent of the electronic properties of R² (see Table 2). Moreover, the R¹ – $E_{pa}(1)$ trend found with complexes **1–3** is no longer observed. Thus, these electrochemical data emphasize that the redox properties of the phenylacetylide complexes **4–14** can be mainly controlled through the variation of the substituting group R¹ which can significantly affect the reduction potential.
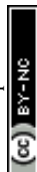
Table 2 Electrochemical data ($E_{pa}(1)$, $E_{pa}(2)$ and $E_{pc}(3)$) for complexes **4–14** (0.5 mM) at a Pt working electrode in CH_2Cl_2/NBu_4PF_6 0.1 M (E/V vs. $Fc^{+/0}$, v = 0.1 V s^{-1}) and DFT-computed electron affinities (EA) and ionization energies (IE) in eV

	1	**2**	**3**	**4**	**5**	**6**	**7**	**8**	**9**	**10**	**11**	**12**	**13**	**14**
$E_{pa}(1)$	0.64	0.61	0.78	0.61	0.54	0.66	0.59	0.51	0.51	0.61	0.54[a]	0.73	0.59	0.53
$E_{pa}(2)$	—	0.93[b]	—	0.88	1.03	0.79	0.73	0.90	0.88	0.84	0.69	0.96	1.02	0.81
$E_{pc}(3)$	−2.00	−1.99	−1.88	−2.04	−2.05	−2.00	−2.02	−2.02	−1.99	−1.99	−2.02	−1.91	−1.92	−1.87
EA	2.50	2.59	2.75	2.52	2.50	2.59	2.54	2.53	2.59	2.59	2.54	2.69	2.68	2.73
IE	6.11	5.70	6.19	5.64	5.34	5.89	5.50	5.27	5.66	5.65	4.99	5.73	5.41	6.00

[a] (0.24 V, NPh_2). [b] A second broad an irreversible peak appears at $E_{pa}(2)$.

Table 3 UV/Vis and PL data of complexes **1–14** in CH_2Cl_2 and in solid state. The λ_{max} values coming from the TD-DFT-simulated spectra are given in brackets below their experimental counterparts

	CH_2Cl_2[a]					KBr	
	UV/Vis λ_{max}, nm (ε, mM^{-1} cm^{-1})	PL λ_{max},[b] nm	τ, µs	Φ_{PL}	Stokes Shift,[c] cm^{-1}	PL λ_{max}, nm	τ, µs
1	237(22.9), 266(28.0), 362 (4.4), 381 (5.8), 410 (4.6) [264, 321, 386]	485, 518, 556 [460]	5.4	0.34[d]	3710	701	15.4
2	267 (23.3), 363 (2.1), 381 (3.3), 448 (4.9) [265, 325, 429]	561, 589 [556]	9.5	0.37[e]	4500	778	15.1
3	263 (28.1), 363 (5.0), 379 (7.4), 404(5.5) [260, 326, 382]	476, 508, 549 [453]	5.6	0.08[d]	3680	—[f]	—[f]
4	270 (44.9), 315 (10.5), 393 (6.6), 426 (4.9) [267, 395]	507, 524 —	5.0	0.07[e]	4670	718	14.0
5	269 (35.3), 322 (7.1), 445 (2.4) [271, 329, 461]	538 [522]	6.7	0.27[d]	3550	717	19.2
6	274 (23.1), 307 (18.6), 390 (2.2) 422 (1.3) [265, 311, 388]	498, 522 [483]	5.6	0.16[d]	4310	732	20.9
7	268 (22.4), 382 (2.1), 451 (3.5) [270, 339, 455]	562, 593 [555]	9.1	0.55[e]	4380	701	13.1
8	269 (86.0), 381 (7.4), 458 (11.3) [272, 327, 360, 479]	572, 590 [562]	9.1	0.81[e]	4350	739	17.3
9	274 (49.0), 306 (42.0), 392 (9.5), 450 (11.9) [265, 312, 427]	561 [548]	7.1	0.35[e]	4400	740	17.9
10	269 (27.1), 336 (4.4), 381 (2.3), 448 (3.2) [265, 334, 427]	561, 592 [549]	12.3	0.52[e]	4500	764	19.3
11	272 (59.9), 317 (51.0), 381 (13.6), 457 (13.8) [267, 330, 383, 503]	605 [568]	—	0.01[e]	5350	741	17.4
12	265 (38.9), 315 (7.6), 393 (6.6), 425 (5.3) [267, 317, 433]	506 [507]	3.4	0.06[e]	3660	—[f]	—[f]
13	266 (30.1), 318 (3.9), 380 (1.5), 445 (1.9) [265, 328, 465]	552 —	4.3	0.18[e]	3500	—[f]	—[f]
14	272 (29.6), 305 (25.8), 373 (6.6), 389 (7.6), 418 (6.1) [263, 309, 385]	495 [494]	3.1	0.02[d]	4010	—[f]	—[f]

[a] All spectra were recorded at room temperature at $c \sim 10^{-5}$ M with deoxygenated solution prepared by bubbling N_2 though the solutions. [b] λ_{exc} = λ_{max}^{abs} of the lowest energy band. [c] Calculated using the less energetic absorption band and the more energetic emission band. [d] Photoluminescence quantum yield (±10%) measured relative to 9,10-bisphenylethynylanthracene in cyclohexane (Φ_{Pl} = 1.00).[59] [e] Photoluminescence quantum yield (±10%) measured relative to Rhodamine 6G in ethanol (Φ_{Pl} = 0.95).[59] [f] No emission detected.

Possibly, the random variation of the oxidation potential $E_{pa}(1)$ with R^2 originates from the different possible orientations of the phenyl ring relative to the cyclometalated ligand, favoring or not conjugation between the two moieties (see computational part).

Photophysical properties

The UV/Vis absorption and photoluminescence (PL) properties of chloro- and alkynyl-platinum complexes **1–14** are summarized in Table 3.

Absorption spectra of chloro-platinum complexes **1–3** are displayed in Fig. 5. These complexes exhibit intense absorption band in the UV region from 250 to 300 nm, assigned to intra-ligand (IL) π–π* transition on the cyclometalated (N^C^N) ligands and less intense bands from 350 to 450 nm attributed in particular to metal to ligand charge transfer (MLCT). For complex **2**, the presence of a methoxy electron-donating group in conjugated position with the platinum atom on the central phenyl ring of the N^C^N ligand induces a significant red-shift of the less energetic absorption band
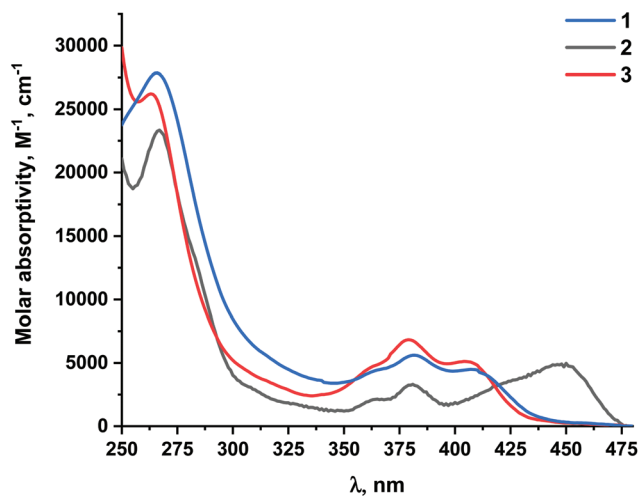
Fig. 5 Absorption spectra of chloro-platinum complexes **1–3** in CH$_2$Cl$_2$ ($c \sim 10^{-5}$ M).

with regards to complex **1** ($\Delta\lambda = 37$ nm), as observed recently in a series of 2-phenylpyrimidine platinum complexes.[60] On the contrary, the presence of a trifluoromethyl electron-withdrawing substituent, in the N^C^N ligand of complex **3** causes a slight blue shift of 6 nm of the same band. Alkynyl-platinum complexes **4–14** exhibit similar absorption profile than their respective chloro-platinum parent complexes, with the lowest-energy absorption band attributed mainly to interligand charge transfer (see computational part). In the series of complexes with methoxy substituted N^C^N ligand, the presence of methoxy electron-donating group on the alkynyl ligands (complex **8**) leads to slight red-shift of the less energetic absorption band with regards to complex **7** (Fig. 6). The same trend is also observed in the two other series of complexes with unsubstituted and trifluoromethyl substituted N^C^N ligand (Fig. S23 and S24†). This red-shift is more pronounced
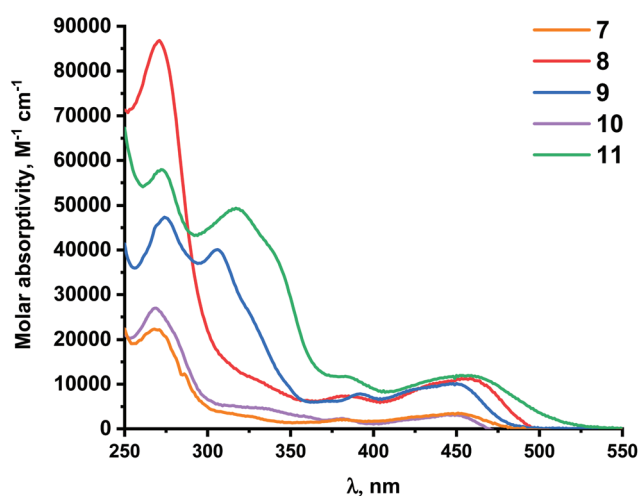
with stronger electron-donating diphenylamino substituent on alkynyl ligand (complex **11**).

All complexes exhibit emission in CH$_2$Cl$_2$ solution with emission lifetimes comprised between 3.1 to 12.3 μs, characteristic of phosphorescence emission. The photoluminescence quantum yield (PLQY) are in some cases rather high (Φ_{PL} up to 0.81), as expected for platinum(II) complexes with N^C^N ligand.[19] The emission spectra of chloro-platinum complexes **1–3** are displayed in Fig. 7. Structured spectra with vibrational spacing of around 1300 cm^{-1} are observed for complexes **1** and **3** as described previously for similar N^C^N complexes.[55] A large red shift of the main emission maxima and longer emission lifetime are displayed by complex **2** with methoxy substituted N^C^N ligand with regard to complex **1** ($\Delta\lambda = 76$ nm). The less structured shape of the emission band of this complex would indicate a lower structural distortion of excited state and could explain the higher PLQY observed.[61] On the other hand, complex **3** with trifluoromethyl substituted N^C^N ligand shows a really similar emission profile than complex **1** with a blue shift of 7–12 nm and reduced PLQY. In the series of alkynyl-platinum complexes **7–11** with methoxy substituted N^C^N ligand, the presence of a methoxy electron-donating group on the alkynyl ligand in complex **8** leads to a slight red shift of the main emission band to 572 nm (Fig. 8). This complex exhibits the best quantum yield of the whole series ($\Phi_{PL} = 0.81$). Diphenylamino group appended on alkynyl ancillary ligand in complex **11** induced a more pronounced red-shift of the position of emission maxima, but the PLQY is dramatically reduced. The replacement of chlorine ligand by a stronger-field ligand such as phenylacetylene ones is known to
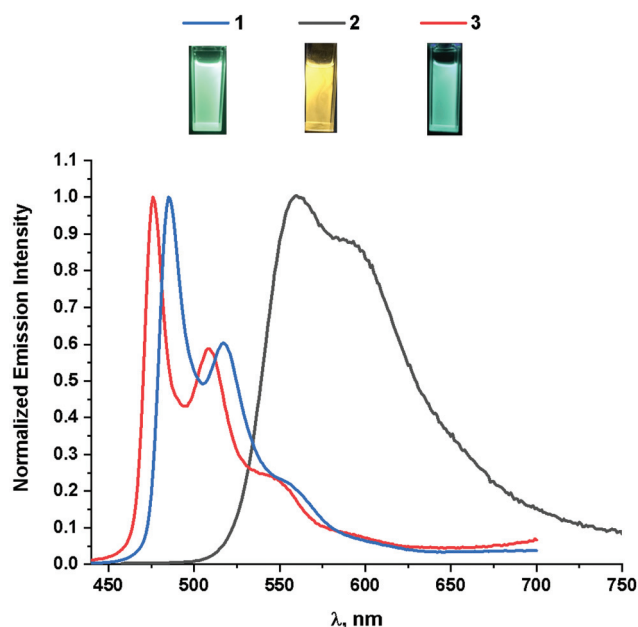

Fig. 7 Normalized emission spectra of chloro-platinum complexes **1–3** in deoxygenated CH$_2$Cl$_2$ solution ($c \sim 10^{-5}$ M). $\lambda_{exc} = \lambda_{max}^{abs}$ of the lowest energy band inset: picture of CH$_2$Cl$_2$ solution taken under UV irradiation.

Fig. 6 Absorption spectra of alkynyl-platinum complexes **7–11** in CH$_2$Cl$_2$ ($c \sim 10^{-5}$ M).
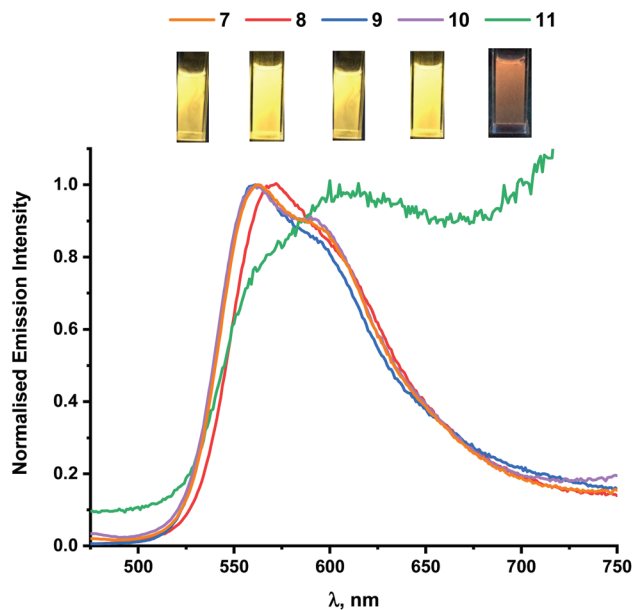
Fig. 8 Normalized emission spectra of alkynyl-platinum complexes **7–11** in deoxygenated CH$_2$Cl$_2$ solution ($c \sim 10^{-5}$ M). $\lambda_{exc} = \lambda_{max}^{abs}$ of the lowest energy band inset: picture of CH$_2$Cl$_2$ solution taken under UV irradiation.

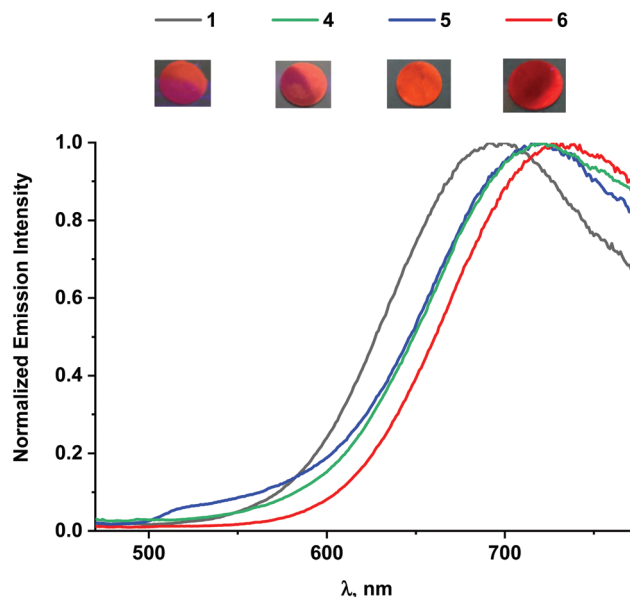**Fig. 9** Normalized emission spectra of complexes **1**, and **4–6** in KBr matrix (2 w%). $\lambda_{exc} = \lambda_{max}^{abs}$ of the lowest energy band in CH$_2$Cl$_2$ solution inset: picture of KBr pellets taken under UV irradiation.

raise the energy of the metal-centered d–d excited state, which is subject to efficient non-radiative decay, well above the emitting triplet state.[61–63] Strong electron-donating diphenylamino or electron-withdrawing cyano groups on the phenylacetylene anciliary ligand in complexes **11** and **9** reduce the PLQY and the highest PLQY are observed with softer electron-donating methoxy group. For the two other series of alkynyl complexes **4–6** and **12–14**, the *p*-anisole alkyne ligand provides the highest PLQY in each case (Fig. S26 and S27†). When compared their analogue complexes based on 1,3-bis(pyrimidin-2-yl)benzene ligand, the complexes **1**, **4**, **12** and **13** exhibit similar emission profile but lower PLQY.[55,64] On the other hand, methoxy substituted chloro-platinum complex **2** exhibits higher PLQY than its pyridine analogue (0.37 *vs.* 0.30).[55]

In solid state, complexes **1**, **2**, **4–11** exhibit red emission with unstructured band attributed to the formation of excimers more than to MMLCT (Fig. 9 and Fig. S27†). Indeed, in solution when the concentration is increased to more than 10^{-4} M a new broad band is observed at respectively 700 and 720 nm for complexes **2** and **8**. On the other hand the absorption and excitation profile are not modified at this concentration and no deviation of the Beer Lamber Law is detected (Fig. S28 and S29†).

Theoretical calculations

Following previous computational studies on related platinum complexes,[31,49,63,65–67] we performed density functional theory (DFT) calculations at the PBE0/Def2-TZVP level were performed to optimize the geometries of chloro- and alkynyl-platinum complexes **1–14**. Solvent (CH$_2$Cl$_2$) effect corrections were included (see Computational details). The 14 optimized struc-

tures are shown in Fig. S30.† Selected computed data are provided in Table 4 and Table S5.† The optimized geometries of **7** and **8** are essentially consistent with their X-ray structures (Table 1). The optimized Pt–N and Pt–C(N^C^N) distances are ~0.5% longer and shorter, respectively, than their X-ray counterparts, whereas the computed Pt-CCR separations are found ~3% shorter than the experimental one. In addition, the phenyl ring makes a larger angle with the N^C^N ligand plane in the X-ray structure of **7** and it is more bent in that of **8**. These differences, which are more pronounced in the case of **7**, can be attributed to the existence of the intermolecular forces existing in the solid state (substantial in the case of **7**, see above), whereas the optimized structures were considered isolated in dichloromethane solution. As a matter of fact, the optimized geometries of **7** and **8** were found nearly planar, as all the investigated complexes, except that of **4**, **6**, **9**, **10**, **11** and **14**. In the case of **11**, the whole molecular framework is planar except that the NPh$_2$ substituent is out-of-plane rotated by ~40° due to steric repulsions. On the other hand, in **4**, **6**, **9**, **10** and **14** the phenyl ring is found perpendicular to the N^C^N ligand. Actually, **6**, **9**, **10** and **14** are the only species bearing an electron accepting group of the phenyl-alkynyl ligand (R^2 = CN, CHO) whereas **4** is unsubstituted. An evaluation of the rotational energy barrier in **4**, **6** and **9** provided values lower than 1 kcal mol^{-1}, indicating nearly free rotation of the phenyl ring in these compounds. Obviously, in these complexes, the Pt center is reluctant to set up the π-type communication between the N^C^N ligand on one side and the phenyl alkynyl group on the other side when R^2 is not a donating group.

Unsurprisingly, the Pt–N distances are almost constant within the whole series (range: 0.006 Å). This is not of course the case for the Pt–C$_{N^C^N}$ distances. The shortest ones, associ-
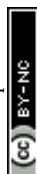
Table 4 Relevant computed data for complexes **1–14**

Compound		1	2	3	4	5	6	7	8	9	10	11	12	13	14
HOMO–LUMO gap (eV)		4.12	3.71	4.15	3.75	3.39	4.01	3.49	3.30	3.72	3.71	3.03	3.60	3.31	3.93
NAO charges	Pt	0.67	0.66	0.68	0.68	0.68	0.68	0.68	0.68	0.68	0.68	0.68	0.69	0.69	0.69
	N	−0.44	−0.44	−0.44	−0.44	−0.44	−0.44	−0.44	−0.44	−0.44	−0.44	−0.43	−0.43	−0.44	−0.44
	$C_{N^{\wedge}C^{\wedge}N}$	−0.05	−0.07	−0.04	−0.13	−0.13	−0.13	−0.16	−0.16	−0.15	−0.15	−0.16	−0.12	−0.12	−0.11
	Cl/C(CR)	−0.73	−0.73	−0.72	−0.40	−0.42	−0.36	−0.40	−0.42	−0.36	−0.36	−0.41	−0.40	−0.42	−0.36
Dipole moment (D)		3.47	4.51	0.70	1.49	1.49	8.78	2.57	0.96	9.77	8.01	2.30	3.01	4.66	4.48

ated with the largest Wiberg bond indices (WBIs), are found for the chloro-platinum derivatives **1–3**. Within the alkynyl-platinum series **4–14**, they lie in a range of 0.006 Å and the shortest correspond to the trifluoromethyl-substituted complexes **12–14**. The Pt-CCR separations vary also within a small range of 0.005 Å, as well as the C≡C distances which are almost constant within the **4–14** series (1.225–1.226 Å). The corresponding WBIs, however, show a larger dispersion (2.704–2.742), indicative of different bond strengths. The larger values corresponds to the cases where there is no donor substituent on the N^C^N ligand together with the presence of the electron donor OCH_3 group on the phenylacetylene ancillary ligand (complexes **5** and **13**). The lowest values correspond to the cases where there is no acceptor substituent on the N^C^N ligand together with the presence of an electro acceptor group on the phenyl ring (complexes **6**, **9** and **10**). Obviously, this latter situation favors conjugation. The natural atomic orbital (NAO) charges show little variations on Pt and N (Table 4). That of the C alkynyl carbon are more dispersed and the lowest negative values correspond to the more conjugated **6**, **9** and **10** complexes. These three compounds have by far the largest dipole moment (Table 4), indicating that the –CN or –CHO substituted phenyl–alkynyl moiety acts as a good acceptor and the N^C^N ligand behaves as a good donor, providing that the latter is not substituted by an electron acceptor group.

The Kohn–Sham MO level energy diagrams of chloro- and alkynyl-platinum complexes **1–14** are shown in Fig. 10 and their HOMOs and LUMOs are plotted in Fig. 11, Fig. S31a and S31b.† The highest HOMOs are those of complexes bearing a donor R^2 substituent (**5**, **8**, **11** and **13**). The lowest HOMOs are those of complexes with no donor substituent (**1**, **3**, **6** and **14**). The LUMO energies are significantly less dispersed in energy and appear more dependent to the nature of R^1 than that of R^2. It results that the lowest HOMO–LUMO gaps are those of complexes with donor R^2 substituents (**8**, **11** and **13**) and the largest HOMO–LUMO gaps are those of compounds with no donor substituent (**1**, **3**, **6** and **14**). The HOMOs of the chloro derivatives **1–3** have a major contribution from the N^C^N ligand, with some Cl and Pt admixture. The same type of N^C^N centered HOMO is found for **9** and **10** (R^1 = H_3CO; R^2 = acceptor). That of all the other complexes can be identified as the π-type HOMO of the substituted phenyl–alkynyl ligand. It is rotated by 90° in the case of the "perpendicular" complexes **4**, **6** and **14** with respect to their "planar" counterparts. In the case of **7–10**, this HOMO gets also some non-negligible contribution from the N^C^N ligand. In all the complexes, the LUMO is N^C^N-localized, as well as the LUMO+1. Rather similar frontier orbital characteristics were found for related chloro- and alkynyl-platinum(II) complexes bearing a N^C^N ligand.[66] The calculated ionization energies (IE; see Computational details) are gathered in Table 2. Their variation across the **1–14** series mainly reflects that of their HOMOs. Surprisingly, no linear relationship could be traced between the recorded E_{pa}(**1**) and neither computed IEs or the HOMO energies. This absence of correlation is likely to be attributed to the irreversible nature of the first oxidation potential. On
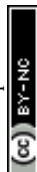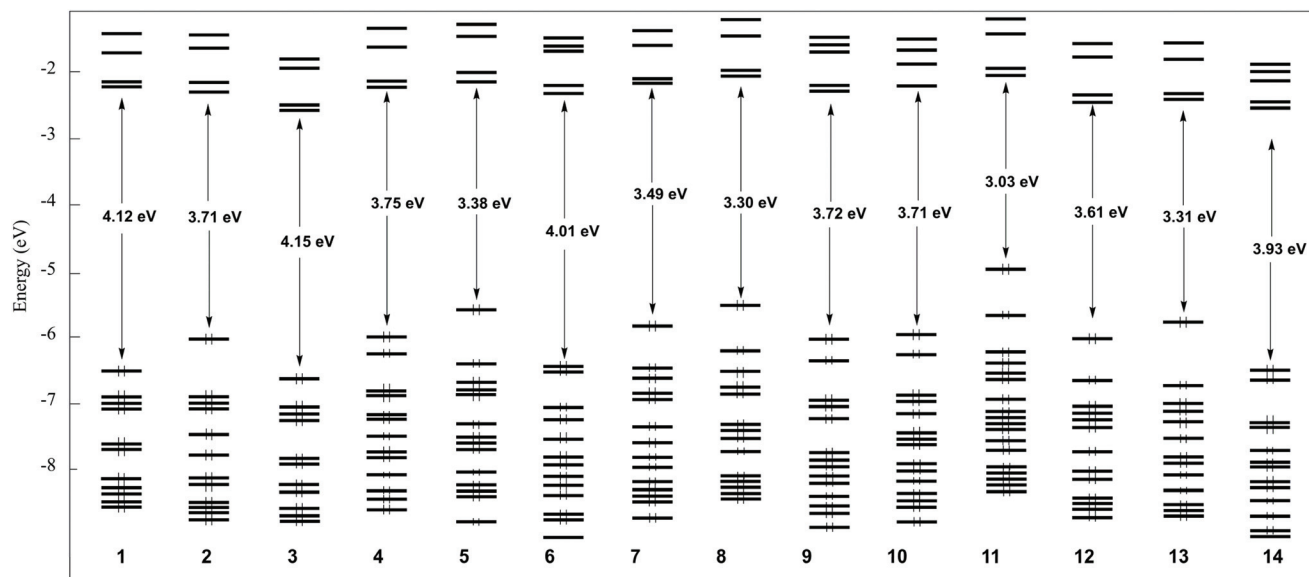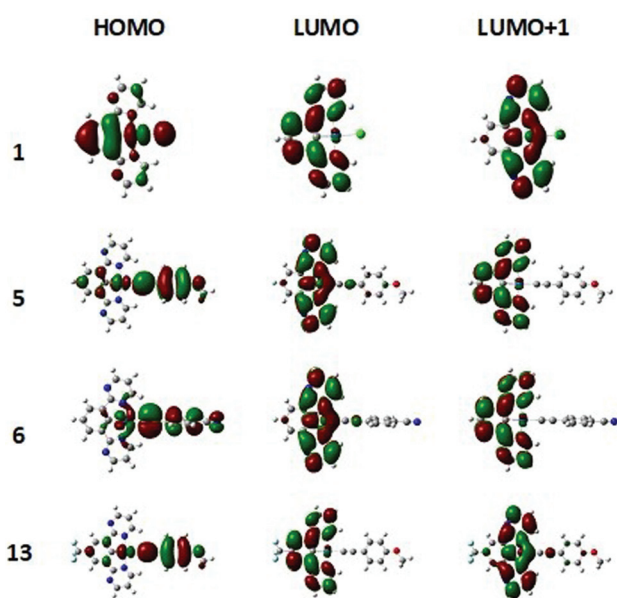
Fig. 10 Kohn–Sham MO diagrams of complexes **1–14**.

Fig. 11 The frontier orbitals of complexes **1**, **5**, **6** and **13**.

the other hand, a good linear correlation can be traced between the electrochemical $E_{pc}(3)$ values and the computed electron affinities (EA; see Computational details), as exemplified by Fig. S32.†

TD-DFT calculations were performed to simulate the UV-vis absorption spectra of complexes **7–14**, which are shown in Fig. S31 and S34.† The simulated and experimental spectra of complexes **1**, **2**, **7** and **8** are plotted together in Fig. S44† to exemplify their rather good consistency. The λ_{max} values of the simulated spectra are given in Table 3, for comparison with the experimental λ_{max}. The major optical transitions contribut-

ing to the simulated band of lowest energy are given in Table S4.† There is an overall good agreement with the experimental data, apart from the fact that the observed weak band of lowest energy of compounds **1–4**, **6** and **14** is not reproduced in the simulations, it should be noted however that in the case of **4** and **6**, the HOMO–LUMO transition is found at ~420 nm (Table S4†), but its modest oscillator strength prevents it to contribute to an individual simulated band of low-energy. In the slightly less stable planar configuration of **4** and **6**, this transition is associated with a slightly higher oscillator strength. In the case of **14**, the HOMO–LUMO transition appears fully forbidden. These results suggest that in the case of complexes **4**, **6** and **14**, the weak band observed at ~420 nm corresponds to the HOMO–LUMO transition (phenyl-akynyl → (N^C^N) charge transfer), the expected oscillator strength of which being underestimated by the calculations in the considered frozen rotational conformations. In the case of complexes **1–3**, the computed absorption band of lowest energy corresponds to the HOMO → LUMO transition and is thus of major intra-(N^C^N) charge transfer character. In the case of the alkynyl complexes **5–14**, it is of HOMO → LUMO and/or HOMO → LUMO+1 nature, thus of major interligand phenyl-akynyl → (N^C^N) charge transfer nature. The phosphorescence data where computed assuming the emissive state being the first excited triplet state, of which the optimized geometries are shown in Fig. S41.† Complexes **4–14** have all their N^C^N ligand and phenyl ring coplanar, compounds **4**, **12** and **14** being in addition bent at the alkynyl carbon bonded to Pt, indicative of an electron-rich phenyl–alkynyl ligand in the excited state. This is consistent with the fact that in all the cases, the involved excited triplet state corresponds to the promotion of a single electron into the LUMO, LUMO+1 or a combination of both. Thus, in the cases of complexes **4–14**, the electron is promoted into a phenyl–alkynyl orbital. The spin

densities of the first excited triplet states, plotted in Fig. S42,† nicely illustrate this view. The simulated emission spectra are shown in Fig. S37–S40,† except that of **4** and **13** that could not be computed, in the case of the former, probably because of the too large structural difference between the ground and excited states. The shapes of the simulated spectra match quite well with those of their experimental counterparts recorded in solution and the agreement between the computed and experimental $\lambda_{\max}$ of the major (first) emission band varies from satisfying to very good (see Table 3). The charge transfers associated with the triplet → singlet emission are illustrated by the plots of the differences between the densities of these two states shown in Fig. S43† and quantified by corresponding transferred fractions of electron q^{CT} over associated spatial extends d^{CT} (see Computational details). From the values of the q^{CT}/d^{CT} couples, the highest quantum yields are expected for compounds **5** and **11–14**, which is obviously not the case (see Table 3). On the other hand, non-radiative decay should not be neglected. It is expected to be, *inter alia*, favored by the amplitude of the structural difference between the triplet and singlet states.[65] From this perspective, complexes **7–10** appear to be among those satisfying both criteria at best (see Fig. S30, S41 and S43†).

Conclusions

In summary, a series of luminescent cyclometallated N^C^N chloro- and alkynyl-platinum(II) complexes based on 1,3-bis(pyrimidin-2-yl)benzene ligands was designed. Their electrochemical and photophysical properties were thoroughly studied experimentally and theoretically with the help of DFT calculation. All compounds are phosphorescent in CH_2Cl_2 solution with emission ranging from green to orange depending on the R^1 and R^2 substituents on the ligands. All complexes, except those with trifluoromethyl substituted ligands exhibit red emission in KBr solid matrix.

For chloro-platinum complexes, the presence of a methoxy group in the central benzene core of the ligand induces a red shift of less energetic absorption and emission band that can be correlated to a reduction of calculated HOMO–LUMO gap. The presence of alkynyl ancillary ligand has a limited influence on absorption and emission spectra except in case of complex **11** with strongly electron-donating diphenylamino R^2 substituent for which a significant red-shift is observed. Reduction potential and LUMO energy are rather independent of the nature of R^2 substituent. In term of emission intensity, the presence of CF_3 electron-withdrawing group as R^1 substituent on the N^C^N ligand has a negative effect. Even if the PLQY of some of these complexes are lower than their analogues based on 1,3-bis(pyrimidin-2-yl)benzene ligand, the presence of OMe groups as both R^1 and R^2 substituents has a beneficial effect on PLQY. In CH_2Cl_2, PLQY up to 0.81 was achieved for complex **8** with $R^1 = R^2 = OMe$, one of the best ever reported for the class of complexes.

These results represent a useful study for the understanding of influence of ligands on the photophysical properties of platinum(II) complexes. Experiments are currently underway to improve solid state emission properties of this family of platinum(II) complexes.

Experimental part

General information

In air- and moisture-sensitive reactions, all glassware was flame-dried. All reactions were conducted under a dry nitrogen atmosphere using Schlenk techniques. The starting materials were purchased from Sigma-Aldrich, TCI or Alfa-Aesar and were used as received. Ligands **15–19**, and complexes **1–2** were prepared as previously reported,[49,55,68,69] whereas new ligand **20** and complexes **3–14** were prepared as described below. The solvents and reactants were used as received except tetrahydrofuran that was distilled under a dry nitrogen atmosphere over sodium and benzophenone. Organic solutions were concentrated under reduced pressure using a rotary evaporator. Thin layer chromatography (TLC) was conducted on pre-coated aluminum sheets with 0.20 mm Merck Alugram SIL G/UV254 with fluorescent indicator UV254 and 0.25 mm Merck silica gel (60-F254). Column chromatography was carried out using Acros silica gel 60 (particle size 63–200 μm) and Macherey Nagel Aluminum neutral oxide 40 (particle size 40–160 μm). Nuclear magnetic resonance (NMR) spectra were acquired at room temperature on a Bruker AC-300 spectrometer (^{1}H at 300 MHz, ^{13}C at 75 MHz,) and referenced as follows: ^{1}H NMR, residual CHCl$_3$ (δ = 7.26 ppm); ^{13}C{^{1}H} NMR, internal CDCl$_3$ (δ = 77.16 ppm). The chemical shifts δ are reported in parts per million relative to TMS (^{1}H, 0.0 ppm) and CDCl$_3$ (^{13}C, 77.16 ppm). The coupling constant J is given in Hz. In the ^{1}H NMR spectra, the following abbreviations are used to describe the peak pattern: s (singlet), d (doublet), dd (doublet of doublet), t (triplet), and m (multiplet). Acidic impurities in CDCl$_3$ were removed by treatment with anhydrous K_2CO_3. IR spectra were recorded on a PerkinElmer spectrum 100 spectrometer with an ATR sampling accessory. High Resolution Mass Spectrometry (HRMS) analyses were performed at the "Centre Régional de Mesures Physiques de l'Ouest" (CRMPO, University of Rennes 1, France) using a Bruker MicroTOFQ II apparatus.

X-ray structure determination

The SCXRD studies of **7** (CCDC 2126978†) and **8** (CCDC 2126979†) were performed on an APEXII, Bruker AXS diffractometer equipped with a CCD plate detector and a Mo-Kα radiation (λ = 0.71073 Å, graphite monochromator). Measurements were done at 150 K. Crystal structures were solved by dual-space algorithm using the SHELXT program,[70] and then refined with full-matrix least-square methods based on F^2 (SHELXL).[71] All non hydrogen atoms were refined with anisotropic atomic displacement parameters. H atoms were finally included in the structural model in their calculated positions, and constrained to ride on the attached carbon atom. Relevant

collection and refinement data for all compounds are given in the ESI.†

Cyclic voltammetry

The electrochemical studies were performed in a glovebox (Jacomex) (O_2 < 1 ppm, H_2O < 1 ppm) with a home-made 3-electrode cell (WE: Pt, RE: Ag wire, CE: Pt). Ferrocene was added at the end of each experiment to determine the redox potential values. The standard potential of the Fc^+/Fc couple in CH_2Cl_2/NBu_4PF_6 was measured experimentally with reference to the standard calomel electrode (SCE): $E°(Fc^+/Fc) = 0.47$ V $vs.$ SCE. The potential of the cell was controlled by an AUTOLAB PGSTAT 100 (Metrohm) potentiostat monitored by the NOVA© software (Metrohm). Dichloromethane was freshly distilled from CaH_2 and kept under Ar in the glovebox. The supporting salt NBu_4PF_6 was synthesized from NBu_4OH (Fluka) and HPF_6 (Aldrich). It was then purified, dried under vacuum for 48 hours at 100 °C, and then kept under N_2 in the glovebox.

Photophysical details

UV/vis absorption spectra were recorded on a Jasco V-650 spectrophotometer. Emission spectra were measured on a Horiba Fluoromax spectrometer. Complexes were excited at their absorption maxima (band of lowest energy) to record the emission spectra in degassed DCM. The emission quantum yields of these complexes were calculated relative to 9,10 – bis (phenylethynyl) anthracene in cyclohexane (Φ_{em} = 1) or Rhodamine 6G in ethanol (Φ_{Pl} = 0.95) as the reference solution.[59] Five diluted solutions (with A > 0.1 at excitation wavelength) are used for studied chromophores and standard. QY is calculated according to the following equation: $\Phi_x =$

$$\Phi_{St} \frac{\text{Grad}_x}{\text{Grad}_{st}} \left(\frac{n_x}{n_{st}}\right)^2$$ where Grad_x and Grad_{St} correspond to the slope of the regression line of integration of the emission band $versus$ the absorbance at the excitation wavelength for the studied chromophore and the standard respectively. The phosphorescence lifetimes measurements of deoxygenated CH_2Cl_2 solutions samples were performed on the same spectrometer in the phosphorimeter mode using xenon flash lamp for excitation. UV-vis and fluorescence spectra were recorded using standard 1 cm quartz cells. Stokes shifts were calculated by considering the lowest energetic absorption and the highest energy emission bands.

Computational details

DFT calculations were carried out using the Gaussian16 package,[72] employing the PBE0 functional,[73–75] together with the Def2-TZVP basis set with relativistic pseudopotentials, from EMSL Basis Set Exchange Library.[76,77] Implicit solvent (chloroform) effects were included through the polarizable continuum model (PCM) approximation, which is routinely used for non-coordinating solvents.[78,79] This level of theory has been shown appropriate in previous investigations on related Pt complexes.[31,80] The optimized geometries were fully

characterized as true minima by analytical frequency calculations (no imaginary values). The geometries obtained from DFT calculations were used to perform natural atomic charge analysis with the NBO 6.0 program.[81] TD-DFT calculations were carried out at the same level of calculations, which has been shown to provide satisfactory results on related investigations.[31,66] Only singlet–singlet transitions were taken into account in these calculations. Only singlet–singlet transitions were taken into account in the TD-DFT calculations. Only the transitions with non-negligible oscillator strengths are discussed in the paper. The graphical SWizard program[82,83] was used for simulating UV-vis spectra. A TD-DFT check did not show any other excited triplet state in the vicinity of the lowest triplet state, except for compound **13** (0.02 eV). Thus, phosphorescence was assumed to occur from the lowest triplet state that was fully optimized at the PBE0/Def2-TZVP level. The phosphorescence emission spectra were computed within the Franck–Condon principle by using the Adiabatic Hessian method[84,85] which takes into account vibrational mode mixing and a proper description of both optimized ground and excited (triplet) states potential energy surfaces. The lowest normal modes in the vibronic treatment were neglected in order to obtain sufficient spectrum progression. We employed the class-based pre-screening to limit the number of terms involved in the vibronic calculation with the following settings: C_{max1} = 70, C_{max2} = 70, N_{max1} = 100 × 108.[86–88] All the vibronic plots were realized using the VMS piece of software.[89] Charge transfers associated with the triplet → singlet emissive transitions were illustrated by plots of the differences between the densities of the excited and ground states and quantified by associated charge transfer values and distance values as defined by Adamo and coworkers.[90–92]

Synthesis

1,3-Di(pyrimidin-2-yl),5-trifluoromethylbenzene **20.** 2-Chloropyrimidine (344 mg, 3 mmol, 3 equiv.) and **17** (398 mg, 1 mmol, 1 equiv.) were introduced in a Schlenk flask. The mixture was degassed by bubbling with nitrogen for 15 minutes. Whereupon toluene (30 mL), K_2CO_3 saturated solution (5 ml) were added. The reaction mixture was stirred under bubbling with nitrogen into the solution for 10 min. Then Pd $(PPh_3)_4$ (174 mg, 15 mol%, 0.15 equiv.) was quickly added. The reaction was stirred under nitrogen at reflux for 48 h. The mixture was diluted with water, and the aqueous layer was extracted with EtOAc (2 × 25 mL). The separated organic phase extracts were dried over $MgSO_4$, filtered and the solvents were evaporated under reduced pressure. The crude product was purified by silica gel column chromatography (petroleum ether to petroleum ether/DCM, 1 : 1, v/v) to give compound **20** as a white crystalline solid in 65% yield (197 mg). NMR (δ (ppm), CDCl$_3$): ^{1}H (300 MHz): 9.75 (s, 1H), 8.94–8.82 (m, 6H), 7.32–7.23 (m, 2H). ^{13}C{^{1}H} NMR (75 MHz, CDCl$_3$): 162.9(C), 157.1(CH), 138.7(C), 131.6(C, $^2J_{CF}$ = 33 Hz), 130.7(CH), 126.7(CH, $^3J_{CF}$ = 4 Hz), 125.6(C, $^1J_{CF}$ = 271 Hz), 119.6(CH). HRMS (ESI) m/z calculated for $C_{15}H_9N_4F_3Na$ [M + Na]$^+$: 325.0672, found: 325.0672 (0 ppm).

Complex 3. A 250 ml Schlenk flask, charged with the tridentate ligand **20** (37 mg, 0.12 mmol, 1 equiv.) and K_2PtCl_4

(50 mg, 0.12 mmol, 1 equiv.) was degassed and back-filled with nitrogen three times. Then glacial acetic acid (15 ml) was introduced into the reaction flask by syringe. The reaction mixture was stirred under nitrogen protection under reflux for 48 h. The precipitate was filtered off and washed subsequently with water, methanol and diethyl ether. The complex **3** was obtained as dark red powder in yield 62% (40 mg). HRMS (ESI) m/z calculated for $C_{15}H_8N_4F_3Na^{195}Pt$ $[M + Na]^+$: 553.9930, found: 553.9932 (0 ppm).

Complex 4. Sodium methoxide (10 mg, 0.18 mmol, 3 equiv.) in methanol (2 mL) was stirred for 15 min. 4-Phenylacetylene (19 mg, 0.18 mmol, 3 equiv.) was added to sodium methoxide solution. The mixture was stirred for 30 min at room temperature. Then complex **1** (28 mg, 0.06 mmol, 1 equiv.) dissolved in solution MeOH/DCM (4 : 1 v/v) was added and the mixture was left for 15 hours at room temperature. Then the solvents were removed, and the crude product was washed with water, methanol, and n-hexane. The complex **4** was obtained as orange powder in 87% yield (28 mg). NMR (δ (ppm), THF-d8): ^{1}H (300 MHz): 9.55 (ddd, $^3J_{HH}$ = 2.2 Hz, $^4J_{HH}$ = 5.7 Hz, $^3J_{HPt}$ = 19.8 Hz, 2H), 8.98 (dd, $^3J_{HH}$ = 2.2 Hz, $^4J_{HH}$ = 4.7 Hz, 2H), 7.87 (d, $^3J_{HH}$ = 7.6 Hz, 2H), 7.39 (s, 1H), 7.38–7.33 (m, 2H), 7.29 (t, $^3J_{HH}$ = 7.6 Hz, 2H), 7.19 (t, $^3J_{HH}$ = 7.6 Hz, 2H), 7.12–7.03 (m, 1H). ^{13}C{^{1}H} NMR (JMOD, 75 MHz, THF-d8): 162.1 (CH), 161.0 (C), 158.5 (CH), 144.8 (C), 136.0 (C), 131.8 (CH), 129.0 (CH), 128.0 (CH), 127.8 (C), 124.9 (CH), 123.7 (CH), 119.9 (CH), 105.6 (C), 105.4 (C). IR (ATR, cm^{-1}): 2083(νC≡C), 1583(νC=C), 1551 (νC=N). HRMS (ESI) m/z calculated for $C_{22}H_{14}N_4Na^{195}Pt$ $[M + Na]^+$: 552.0759, found: 552.0761 (0 ppm).

Complex 5. The complex was synthesized according to a similar procedure employed for complex **4**, except 4-ethynylanisole (24 mg, 0.18 mmol) was used in place of 4-phenylacetylene. The complex **5** was obtained as orange powder in 93% yield (33 mg). NMR (δ (ppm), THF-d8): ^{1}H (300 MHz): 9.56 (ddd, $^3J_{HH}$ = 2.3 Hz, $^4J_{HH}$ = 5.7 Hz, $^3J_{HPt}$ = 19.2 Hz, 2H), 8.97 (dd, $^3J_{HH}$ = 2.5 Hz, $^4J_{HH}$ = 4.6 Hz, 2H), 7.85 (d, $^3J_{HH}$ = 7.6 Hz, 2H), 7.45–7.14 (m, 5H), 6.77 (d, $^3J_{HH}$ = 8.4 Hz, 2H), 3.75 (s, 3H). ^{13}C{^{1}H} NMR (JMOD, 75 MHz, THF-d8): 162.2 (CH), 160.1 (C), 158.5 (CH), 138.1 (C), 132.7 (CH), 129.0 (CH), 128.0 (C), 123.6 (CH), 120.2 (C), 119.8 (CH), 113.6 (CH), 112.0 (C), 109.6 (C), 54.9 (OCH$_3$). IR (ATR, cm^{-1}): 2084(νC≡C), 1578(νC=C), 1549(νC=N), 1046(νC=O). HRMS (ESI) m/z calculated for $C_{23}H_{16}N_4ONa^{195}Pt$ $[M + Na]^+$: 582.0864, found: 582.0868 (1 ppm).

Complex 6. The complex was synthesized according to a similar procedure employed for complex **4**, except 4-ethynylbenzonitrile (23 mg, 0.18 mmol) was used in place of 4-phenylacetylene. The complex **6** was obtained as orange powder in 84% yield (28 mg). NMR (δ (ppm), THF-d8): ^{1}H (300 MHz): 9.45 (ddd, $^3J_{HH}$ = 2.2 Hz, $^4J_{HH}$ = 5.7 Hz, $^3J_{HPt}$ = 19.2 Hz, 2H), 8.98 (dd, $^3J_{HH}$ = 1.8 Hz, $^4J_{HH}$ = 4.3 Hz, 2H), 7.85 (d, $^3J_{HH}$ = 7.6 Hz, 2H), 7.58–7.54 (m, 2H), 7.52–7.48 (m, 2H), 7.38–7.34 (m, 2H), 7.31–7.26 (m, 1H). IR (ATR, cm^{-1}): 2219(νC≡N), 2080 (νC≡C), 1582(νC=C), 1553(νC=N). HRMS (ESI) m/z calculated for $C_{23}H_{13}N_5Na^{195}Pt$ $[M + Na]^+$: 577.0711, found: 577.0712 (0 ppm).

Complex 7. The complex was synthesized according to a similar procedure employed for complex **4**, except complex **2** (30 mg, 0.06 mmol) was used in place of complex **1**. The complex **7** was obtained as orange powder in 57% yield (20 mg). NMR (δ (ppm), CDCl$_3$): ^{1}H (300 MHz): 9.54 (ddd, $^3J_{HH}$ = 2.3 Hz, $^4J_{HH}$ = 5.6 Hz, $^3J_{HPt}$ = 23.1 Hz, 2H), 8.91 (dd, $^3J_{HH}$ = 2.3 Hz, $^4J_{HH}$ = 4.8 Hz, 2H), 7.54 (m, 4H), 7.36–7.27 (m, 2H), 7.23–7.14 (m, 3H), 3.92 (s, 1H). ^{13}C{^{1}H} NMR (JMOD, 75 MHz, CDCl$_3$) 161.9(CH), 157.9(CH), 157.1(C), 151.2(C), 145.8(C), 131.8(CH), 128.2(CH), 125.7(CH), 120.6(C), 119.6(C), 119.1 (CH), 115.7(CH), 115.4(C), 112.7(C), 56.3(OCH$_3$). IR (ATR, cm^{-1}): 2085(νC≡C), 1578(νC=C), 1549(νC=N), 1046(νC–O). HRMS (ESI) m/z calculated for $C_{23}H_{16}N_4ONa^{195}Pt$ $[M + Na]^+$: 582.0864, found: 582.0866 (0 ppm).

Complex 8. The complex was synthesized according to a similar procedure employed for complex **4**, except complex **2** (30 mg, 0.06 mmol) and 4-ethynylanisole (24 mg, 0.18 mmol) were used in place of complex **1** and 4-phenylacetylene. The complex **8** was obtained as yellow powder in 73% yield (26 mg). NMR (δ (ppm), CDCl$_3$): ^{1}H (300 MHz): 9.56 (ddd, $^3J_{HH}$ = 2.3 Hz, $^4J_{HH}$ = 5.7 Hz, $^3J_{HPt}$ = 21.6 Hz, 2H), 8.91 (dd, $^3J_{HH}$ = 2.3 Hz, $^4J_{HH}$ = 4.8 Hz, 2H), 7.54 (s, 2H), 7.48 (d, $^4J_{HH}$ = 8.8 Hz, 2H), 7.19 (t, 2H), 6.84 (d, $^3J_{HH}$ = 8.9 Hz, 2H), 3.92 (s, 3H), 3.82 (s, 3H). ^{13}C{^{1}H} NMR (JMOD, 75 MHz, CDCl$_3$) 162.6(C), 161.9 (CH), 158.2(C), 157.8(CH), 148.2(C), 133.9(C), 132.9(CH), 119.1 (CH), 116.4(C), 115.6(CH), 115.2(C), 113.8(CH), 113.4(C), 112.2 (C), 56.3(OCH$_3$), 55.4(OCH$_3$). IR (ATR, cm^{-1}): 2083(νC≡C), 1578(νC=C), 1551(νC=N), 1044(νC–O). HRMS m/z calculated for $C_{24}H_{18}N_4O_2Na^{195}Pt$ $[M + Na]^+$: 612.0970, found: 612.0977 (1 ppm).

Complex 9. The complex was synthesized by according to a similar procedure employed for complex **4**, except complex **2** (30 mg, 0.06 mmol) and 4-ethynylbenzonitrile (23 mg, 0.18 mmol) were used in place of complex **1** and 4-phenylacetylene. The complex **9** was obtained as yellow powder in 91% yield (32 mg). NMR (δ (ppm), CDCl$_3$): ^{1}H (300 MHz): 9.41 (ddd, $^3J_{HH}$ = 2.3 Hz, $^4J_{HH}$ = 5.7 Hz, $^3J_{HPt}$ = 19.5 Hz, 2H), 8.92 (dd, $^3J_{HH}$ = 2.3 Hz, $^4J_{HH}$ = 4.8 Hz, 2H), 7.55 (s, 4H), 7.52 (s, 2H), 7.19 (dd, $^3J_{HH}$ = 4.9 Hz, $^3J_{HH}$ = 5.7 Hz, 2H), 3.92 (s, 3H). IR (ATR, cm^{-1}): 2224(νC≡N), 2090(νC≡C), 1577(νC=C), 1552 (νC=N), 1046(νC–O). HRMS (ESI) m/z calculated for $C_{24}H_{15}N_5ONa^{195}Pt$ $[M + Na]^+$: 607.0817, found: 607.0820 (0 ppm).

Complex 10. The complex was synthesized by method B according to a similar procedure employed for complex **4**, except complex **2** (30 mg, 0.06 mmol) and 4-ethynylbenzaldehyde (24 mg, 0.18 mmol) were used in place of complex **1** and 4-phenylacetylene. The complex **10** was obtained as yellow powder in 60% yield (22 mg). NMR (δ (ppm), CDCl$_3$): ^{1}H (300 MHz): 9.98 (s, 1H), 9.41 (ddd, $^3J_{HH}$ = 2.3 Hz, $^4J_{HH}$ = 5.7 Hz, $^3J_{HPt}$ = 22.8 Hz, 2H), 8.89 (dd, $^3J_{HH}$ = 2.3 Hz, $^4J_{HH}$ = 4.8, 2H), 7.80 (d, $^3J_{HH}$ = 8.3 Hz, 2H), 7.62 (d, $^3J_{HH}$ = 8.2 Hz, 2H), 7.48 (s, 2H), 7.17 (t, 2H), 3.92 (s, 3H). ^{13}C{^{1}H} NMR (JMOD, 75 MHz, CDCl$_3$) 191.7(CHO), 176.4(C), 166.9(C), 161.6(CH), 158.1(C), 157.8(CH), 140.4(C), 133.5(C), 132.2(CH), 129.8(CH), 126.9 (CH), 125.9(C), 119.1(CH), 115.5(CH), 112.2(C), 56.19(OCH$_3$).

IR (ATR, cm^{-1}): 2085(νC≡C), 1686(νC=O), 1577(νC=C), 1551 (νC=N), 1046(νC–O). HRMS (ESI) *m/z* calculated for C$_{24}$H$_{16}$N$_4$O$_2$Na^{195}Pt [M + Na]$^+$: 610.0813, found: 610.0816 (0 ppm).

Complex 11. The complex was synthesized by method B according to a similar procedure employed for complex **4**, except complex **2** (30 mg, 0.06 mmol) and 4-ethynyltriphenyl-amine (49 mg, 0.18 mmol) were used in place of complex **1** and 4-phenylacetylene. The complex **11** was obtained as orange powder in 80% yield (35 mg). NMR (δ (ppm), CDCl$_3$): ^{1}H (300 MHz): 9.56 (ddd, $^3J_{HH}$ = 2.2 Hz, $^4J_{HH}$ = 5.6 Hz, $^3J_{HPt}$ = 22.2 Hz, 2H), 8.92 (dd, $^3J_{HH}$ = 2.3 Hz, $^4J_{HH}$ = 4.8 Hz, 2H), 7.55 (s, 2H), 7.43 (d, $^3J_{HH}$ = 8.4 Hz, 2H), 7.26 (s, 2H), 7.25 (s, 2H), 7.23–7.16 (m, 3H), 7.10 (d, $^3J_{HH}$ = 7.6 Hz, 3H), 7.00 (dd, $^3J_{HH}$ = 5.6 Hz, $^4J_{HH}$ = 7.8 Hz, 4H), 3.92 (s, 3H). IR (ATR, cm^{-1}): 2087 (νC≡C), 1579(νC=C), 1551(νC=N). HRMS (ESI) *m/z* calculated for C$_{35}$H$_{25}$N$_5$ONa^{195}Pt [M + Na]$^+$: 749.1599, found: 749.1603 (0 ppm).

Complex 12. The complex was synthesized according to a similar procedure employed for complex **4**, except complex **3** (32 mg, 0.06 mmol) was used in place of complex **1**. The complex **12** was obtained as green powder in 96% yield (35 mg). NMR (δ (ppm), CDCl$_3$): ^{1}H (300 MHz): 9.46 (ddd, $^3J_{HH}$ = 2.2 Hz, $^4J_{HH}$ = 5.7 Hz, $^3J_{HPt}$ = 21 Hz, 2H), 8.90 (dd, $^3J_{HH}$ = 2.2 Hz, $^4J_{HH}$ = 4.8 Hz, 2H), 8.01 (s, 2H), 7.48 (d, $^3J_{HH}$ = 7.3 Hz, 2H), 7.31 (t, $^3J_{HH}$ = 7.5 Hz, 2H), 7.25–7.16 (m, 3H). ^{13}C{^{1}H} NMR (JMOD, 75 MHz, CDCl$_3$) 179.7 (C), 175.1 (C), 161.5 (CH), 157.8 (CH), 140.0 (C), 132.6 (CH), 131.8 (CH), 129.3 (CH), 128.2 (CH), 128.0 (C), 126.4 (C), 125.8 (CH), 125.4 (CH), 123.0 (C), 119.6 (CH), 112.8 (C). IR (ATR, cm^{-1}): 2086(νC≡C), 1585(νC=C), 1553(νC=N). HRMS (ESI) *m/z* calculated for C$_{23}$H$_{13}$N$_4$Na^{195}Pt [M + Na]$^+$: 620.0632, found: 620.0633 (0 ppm).

Complex 13. The complex was synthesized according to a similar procedure employed for complex **4**, except complex **3** (32 mg, 0.06 mmol) and 4-ethynylanisole (24 mg, 0.18 mmol) were used in place of complex **1** and 4-phenylacetylene. The complex **13** was obtained as dark red powder in 96% yield (37 mg). NMR (δ (ppm), CDCl$_3$): ^{1}H (300 MHz): 9.41 (ddd, $^3J_{HH}$ = 2.1 Hz, $^4J_{HH}$ = 5.6 Hz, $^3J_{HPt}$ = 18.9 Hz, 2H), 8.86 (dd, $^3J_{HH}$ = 2.1 Hz, $^4J_{HH}$ = 4.6 Hz, 2H), 7.95 (s, 2H), 7.40 (d, $^3J_{HH}$ = 8.6 Hz, 2H), 7.14 (t, $^3J_{HH}$ = 5.2 Hz, 2H), 6.85 (d, $^3J_{HH}$ = 8.6 Hz, 2H), 3.84 (s, 3H). ^{13}C{^{1}H} NMR (JMOD, 75 MHz, CDCl$_3$) 161.7(CH), 157.9 (CH), 153.9(C), 149.2(C), 140.1(C), 132.9(CH), 129.2(C), 126.6 (C), 125.7(CH), 119.7(CH), 113.8(CH), 112.8(C), 104.9(C), 98.3 (C), 55.5(OCH3). IR (ATR, cm^{-1}): 2094(νC≡C), 1582(νC=C), 1505(νC=N), 1060(νC–O). HRMS (ESI) *m/z* calculated for C$_{24}$H$_{15}$N$_4$OF$_3$Na^{195}Pt [M + Na]$^+$: 650.0738, found: 650.0734 (1 ppm).

Complex 14. The complex was synthesized according to a similar procedure employed for complex **4**, except complex **3** (32 mg, 0.06 mmol) and 4-ethynylbenzonitrile (23 mg, 0.18 mmol) were used in place of complex **1** and 4-phenyl-acetylene. The complex **14** was obtained as green powder in 72% yield (27 mg). NMR (δ (ppm), CDCl$_3$): ^{1}H (300 MHz): 9.44 (ddd, $^3J_{HH}$ = 2.3 Hz, $^4J_{HH}$ = 5.6 Hz, $^3J_{HPt}$ = 20.1 Hz, 2H), 8.99 (dd, $^3J_{HH}$ = 2.2 Hz, $^4J_{HH}$ = 4.8 Hz, 2H), 8.12 (s, 2H), 7.56 (q,

$^3J_{HH}$ = 8.5 Hz, 4H), 7.35–7.26 (m, 2H). IR (ATR, cm^{-1}): 2020 (νC≡N), 2089(νC≡C), 1593(νC=C), 1552(νC=N). HRMS (ESI) *m/z* calculated for C$_{24}$H$_{12}$N$_5$F$_3$Na^{195}Pt [M + Na]$^+$: 645.0585, found: 645.0590 (1 ppm).

Conflicts of interest

There are no conflicts of interest to declare.

Acknowledgements

Notes and references

1 W. T. Eckenhoff and R. Eisenberg, *Dalton Trans.*, 2012, **41**, 13004.

2 D. M. Schultz and T. P. Yoon, *Science*, 2014, **343**, 1239176–1239176.

3 J. Twilton, C. Le, P. Zhang, M. H. Shaw, R. W. Evans and D. W. C. MacMillan, *Nat. Rev. Chem.*, 2017, **1**, 0052.

4 J. He, Z.-Q. Bai, P.-F. Yuan, L.-Z. Wu and Q. Liu, *ACS Catal.*, 2021, **11**, 446–455.

5 M. Mauro, A. Aliprandi, D. Septiadi, N. S. Kehr and L. De Cola, *Chem. Soc. Rev.*, 2014, **43**, 4144–4166.

6 V. W.-W. Yam and A. S.-Y. Law, *Coord. Chem. Rev.*, 2020, **414**, 213298.

7 K. K.-W. Lo, *Acc. Chem. Res.*, 2020, **53**, 32–44.

8 S.-W. Lai and C.-M. Che, in *Transition Metal and Rare Earth Compounds*, Springer Berlin Heidelberg, Berlin, Heidelberg, 2004, vol. 241, pp. 27–63.

9 H. Yersin, A. F. Rausch, R. Czerwieniec, T. Hofbeck and T. Fischer, *Coord. Chem. Rev.*, 2011, **255**, 2622–2652.

10 P.-T. Chou, Y. Chi, M.-W. Chung and C.-C. Lin, *Coord. Chem. Rev.*, 2011, **255**, 2653–2665.

11 L. Xiao, Z. Chen, B. Qu, J. Luo, S. Kong, Q. Gong and J. Kido, *Adv. Mater.*, 2011, **23**, 926–952.

12 M. A. Baldo, D. F. O'Brien, Y. You, A. Shoustikov, S. Sibley, M. E. Thompson and S. R. Forrest, *Nature*, 1998, **395**, 151–154.

13 M. A. Baldo, S. Lamansky, P. E. Burrows, M. E. Thompson and S. R. Forrest, *Appl. Phys. Lett.*, 1999, **75**, 4–6.

14 C. Adachi, M. A. Baldo, S. R. Forrest and M. E. Thompson, *Appl. Phys. Lett.*, 2000, **77**, 904–906.

15 M. Ikai, S. Tokito, Y. Sakamoto, T. Suzuki and Y. Taga, *Appl. Phys. Lett.*, 2001, **79**, 156–158.

16 H. Sasabe and J. Kido, *Eur. J. Org. Chem.*, 2013, 7653–7663.

17 B. Minaev, G. Baryshnikov and H. Agren, *Phys. Chem. Chem. Phys.*, 2014, **16**, 1719–1758.

18 P. Rajakannu, H. S. Kim, W. Lee, A. Kumar, M. H. Lee and S. Yoo, *Inorg. Chem.*, 2020, **59**, 12461–12470.

19 C. Cebrián and M. Mauro, *Beilstein J. Org. Chem.*, 2018, **14**, 1459–1481.

20 M. Z. Shafikov, P. Pander, A. V. Zaytsev, R. Daniels, R. Martinscroft, F. B. Dias, J. A. G. Williams and V. N. Kozhevnikov, *J. Mater. Chem. C*, 2021, **9**, 127–135.

21 H. Shahroosvand, L. Najafi, A. Sousaraei, E. Mohajerani and M. Janghouri, *J. Mater. Chem. C*, 2013, **1**, 6970.

22 J.-L. Liao, Y. Chi, Y.-D. Su, H.-X. Huang, C.-H. Chang, S.-H. Liu, G.-H. Lee and P.-T. Chou, *J. Mater. Chem. C*, 2014, **2**, 6269.

23 M.-C. Tang, M.-Y. Chan and V. W.-W. Yam, *Chem. Rev.*, 2021, **121**, 7249–7279.

24 W.-Y. Wong and C.-L. Ho, *Coord. Chem. Rev.*, 2009, **253**, 1709–1758.

25 X. Yang, G. Zhou and W.-Y. Wong, *Chem. Soc. Rev.*, 2015, **44**, 8484–8575.

26 L. Bischoff, C. Baudequin, C. Hoarau and E. P. Urriolabeitia, in *Advances in Organometallic Chemistry*, Elsevier, 2018, vol. 69, pp. 73–134.

27 E. Kabir, Y. Wu, S. Sittel, B.-L. Nguyen and T. S. Teets, *Inorg. Chem. Front.*, 2020, **7**, 1362–1373.

28 Y. Chi and P.-T. Chou, *Chem. Soc. Rev.*, 2010, **39**, 638–655.

29 S. Huo, J. Carroll and D. A. K. Vezzu, *Asian J. Org. Chem.*, 2015, **4**, 1210–1245.

30 P. Pander, G. Turnbull, A. V. Zaytsev, F. B. Dias and V. N. Kozhevnikov, *Dyes Pigm.*, 2021, **184**, 108857.

31 M. Hruzd, S. Gauthier, J. Boixel, S. Kahlal, N. le Poul, J.-Y. Saillard, S. Achelle and F. Robin-le Guen, *Dyes Pigm.*, 2021, 109622.

32 Y. Unger, D. Meyer, O. Molt, C. Schildknecht, I. Münster, G. Wagenblast and T. Strassner, *Angew. Chem., Int. Ed.*, 2010, **49**, 10214–10216.

33 T. Fleetham, Z. Wang and J. Li, *Org. Electron.*, 2012, **13**, 1430–1435.

34 D. A. K. Vezzu, J. C. Deaton, J. S. Jones, L. Bartolotti, C. F. Harris, A. P. Marchetti, M. Kondakova, R. D. Pike and S. Huo, *Inorg. Chem.*, 2010, **49**, 5107–5119.

35 S. C. F. Kui, P. K. Chow, G. S. M. Tong, S.-L. Lai, G. Cheng, C.-C. Kwok, K.-H. Low, M. Y. Ko and C.-M. Che, *Chem. – Eur. J.*, 2013, **19**, 69–73.

36 E. Turner, N. Bakken and J. Li, *Inorg. Chem.*, 2013, **52**, 7344–7351.

37 J. Kalinowski, V. Fattori, M. Cocchi and J. A. G. Williams, *Coord. Chem. Rev.*, 2011, **255**, 2401–2425.

38 G.-J. Zhou, Q. Wang, W.-Y. Wong, D. Ma, L. Wang and Z. Lin, *J. Mater. Chem.*, 2009, **19**, 1872.

39 M. Tanaka and H. Mori, *J. Phys. Chem. C*, 2014, **118**, 12443–12449.

40 H. Tsujimoto, S. Yagi, Y. Honda, H. Terao, T. Maeda, H. Nakazumi and Y. Sakurai, *J. Lumin.*, 2010, **130**, 217–221.

41 M. Hissler, J. E. McGarrah, W. B. Connick, D. K. Geiger, S. D. Cummings and R. Eisenberg, *Coord. Chem. Rev.*, 2000, **208**, 115–137.

42 S. C. F. Kui, F.-F. Hung, S.-L. Lai, M.-Y. Yuen, C.-C. Kwok, K.-H. Low, S. S.-Y. Chui and C.-M. Che, *Chem. – Eur. J.*, 2012, **18**, 96–109.

43 W. Zhang, J. Wang, Y. Xu, W. Li and W. Shen, *J. Organomet. Chem.*, 2017, **836–837**, 26–33.

44 S.-W. Lai, M. C.-W. Chan, T.-C. Cheung, S.-M. Peng and C.-M. Che, *Inorg. Chem.*, 1999, **38**, 4046–4055.

45 K. Wong and V. Yam, *Coord. Chem. Rev.*, 2007, **251**, 2477–2488.

46 K. M.-C. Wong and V. W.-W. Yam, *Acc. Chem. Res.*, 2011, **44**, 424–434.

47 V. W.-W. Yam, V. K.-M. Au and S. Y.-L. Leung, *Chem. Rev.*, 2015, **115**, 7589–7728.

48 C.-H. Tseng, M. A. Fox, J.-L. Liao, C.-H. Ku, Z.-T. Sie, C.-H. Chang, J.-Y. Wang, Z.-N. Chen, G.-H. Lee and Y. Chi, *J. Mater. Chem. C*, 2017, **5**, 1420–1435.

49 X. Li, J. Hu, Y. Wu, R. Li, D. Xiao, W. Zeng, D. Zhang, Y. Xiang and W. Jin, *Dyes Pigm.*, 2017, **141**, 188–194.

50 E. Rossi, A. Colombo, C. Dragonetti, D. Roberto, R. Ugo, A. Valore, L. Falciola, P. Brulatti, M. Cocchi and J. A. G. Williams, *J. Mater. Chem.*, 2012, **22**, 10650.

51 W. Lu, B.-X. Mi, M. C. W. Chan, Z. Hui, C.-M. Che, N. Zhu and S.-T. Lee, *J. Am. Chem. Soc.*, 2004, **126**, 4958–4971.

52 W. Wu, D. Huang, X. Yi and J. Zhao, *Dyes Pigm.*, 2013, **96**, 220–231.

53 W. Zhang, Y. Luo, Y. Xu, L. Tian, M. Li, R. He and W. Shen, *Dalton Trans.*, 2015, **44**, 18130–18137.

54 E. S.-H. Lam, D. P.-K. Tsang, W. H. Lam, A. Y.-Y. Tam, M.-Y. Chan, W.-T. Wong and V. W.-W. Yam, *Chem. – Eur. J.*, 2013, **19**, 6385–6397.

55 Z. Wang, E. Turner, V. Mahoney, S. Madakuni, T. Groy and J. Li, *Inorg. Chem.*, 2010, **49**, 11276–11286.

56 E. Rossi, A. Colombo, C. Dragonetti, S. Righetto, D. Roberto, R. Ugo, A. Valore, J. A. G. Williams, M. G. Lobello, F. De Angelis, S. Fantacci, I. Ledoux-Rak, A. Singh and J. Zyss, *Chem. – Eur. J.*, 2013, **19**, 9875–9883.

57 C. F. Harris, D. A. K. Vezzu, L. Bartolotti, P. D. Boyle and S. Huo, *Inorg. Chem.*, 2013, **52**, 11711–11722.

58 J. Schneider, P. Du, P. Jarosz, T. Lazarides, X. Wang, W. W. Brennessel and R. Eisenberg, *Inorg. Chem.*, 2009, **48**, 4306–4316.

59 M. Taniguchi and J. S. Lindsey, *Photochem. Photobiol.*, 2018, **94**, 290–327.

60 M. Fecková, S. Kahlal, T. Roisnel, J.-Y. Saillard, J. Boixel, M. Hruzd, P. le Poul, S. Gauthier, F. Robin le Guen, F. Bureš and S. Achelle, *Eur. J. Inorg. Chem.*, 2021, **2021**, 1592–1600.

61 K. Li, G. S. Ming Tong, Q. Wan, G. Cheng, W.-Y. Tong, W.-H. Ang, W.-L. Kwong and C.-M. Che, *Chem. Sci.*, 2016, **7**, 1653–1673.

62 S. J. Farley, D. L. Rochester, A. L. Thompson, J. A. K. Howard and J. A. G. Williams, *Inorg. Chem.*, 2005, **44**, 9690–9703.

63 G. S.-M. Tong and C.-M. Che, *Chem. – Eur. J.*, 2009, **15**, 7225–7237.

64 Y. Chen, K. Li, W. Lu, S.-Y. Chui, C.-W. Ma and C.-M. Che, *Angew. Chem., Int. Ed.*, 2009, **48**, 9909–9913.

65 W. Shen, W. Zhang and C. Zhu, *Phys. Chem. Chem. Phys.*, 2017, **19**, 23532–23540.

66 R. J. Ortiz, J. D. Braun, J. A. G. Williams and D. E. Herbert, *Inorg. Chem.*, 2021, **60**, 16881–16894.

67 M. Xie and W. Lu, *Dalton Trans.*, 2019, **48**, 1275–1283.

68 A. M. Mfuh, V. T. Nguyen, B. Chhetri, J. E. Burch, J. D. Doyle, V. N. Nesterov, H. D. Arman and O. V. Larionov, *J. Am. Chem. Soc.*, 2016, **138**, 8408–8411.

69 J. Tasseroul, M. M. Lorenzo-Garcia, J. Dosso, F. Simon, S. Velari, A. De Vita, P. Tecilla and D. Bonifazi, *J. Org. Chem.*, 2020, **85**, 3454–3464.

70 G. M. Sheldrick, SHELXT - Integrated Space-group and Crystal-structure Determination, *Acta Crystallogr., Sect. A: Found. Adv.*, 2015, **71**, 3–8.

71 G. M. Sheldrick, Crystal Structure Refinement with SHELXL, *Acta Crystallogr., Sect. C: Struct. Chem.*, 2015, **71**, 3–8.

72 M. J. Frisch, G. W. Trucks, H. B. Schlegel, G. E. Scuseria, M. A. Robb, J. R. Cheeseman, G. Scalmani, V. Barone, G. A. Petersson, H. Nakatsuji, X. Li, M. Caricato, A. V. Marenich, J. Bloino, B. G. Janesko, R. Gomperts, B. Mennucci, H. P. Hratchian, J. V. Ortiz, A. F. Izmaylov, J. L. Sonnenberg, D. Williams-Young, F. Ding, F. Lipparini, F. Egidi, J. Goings, B. Peng, A. Petrone, T. Henderson, D. Ranasinghe, V. G. Zakrzewski, J. Gao, N. Rega, G. Zheng, W. Liang, M. Hada, M. Ehara, K. Toyota, R. Fukuda, J. Hasegawa, M. Ishida, T. Nakajima, Y. Honda, O. Kitao, H. Nakai, T. Vreven, K. Throssell, J. A. Montgomery, Jr., J. E. Peralta, F. Ogliaro, M. J. Bearpark, J. J. Heyd, E. N. Brothers, K. N. Kudin, V. N. Staroverov, T. A. Keith, R. Kobayashi, J. Normand, K. Raghavachari, A. P. Rendell, J. C. Burant, S. S. Iyengar, J. Tomasi, M. Cossi, J. M. Millam, M. Klene, C. Adamo, R. Cammi, J. W. Ochterski, R. L. Martin, K. Morokuma, O. Farkas, J. B. Foresman and D. J. Fox, *Gaussian 16, Revision B.01*, Gaussian, Inc., Wallingford CT, 2016.

73 J. P. Perdew, K. Burke and M. Ernzerhof, *Phys. Rev. Lett.*, 1996, **77**, 3865–3868.

74 J. P. Perdew, K. Burke and M. Ernzerhof, *Phys. Rev. Lett.*, 1997, **78**, 1396–1396.

75 C. Adamo and V. Barone, *J. Chem. Phys.*, 1999, **110**, 6158–6170.

76 A. Schäfer, H. Horn and R. Ahlrichs, *J. Chem. Phys.*, 1992, **97**, 2571–2577.

77 A. Schäfer, C. Huber and R. Ahlrichs, *J. Chem. Phys.*, 1994, **100**, 5829–5835.

78 J. Tomasi, R. Cammi, B. Mennucci, C. Cappelli and S. Corni, *Phys. Chem. Chem. Phys.*, 2002, **4**, 5697–5712.

79 J. Tomasi, B. Mennucci and R. Cammi, *Chem. Rev.*, 2005, **105**, 2999–3093.

80 S. Gauthier, A. Porter, S. Achelle, T. Roisnel, V. Dorcet, A. Barsella, N. Le Poul, P. Guevara Level, D. Jacquemin and F. Robin-Le Guen, *Organometallics*, 2018, **37**, 2232–2244.

81 E. D. Glendening, J. K. Badenhoop, A. E. Reed, J. E. Carpenter, J. A. Bohmann, C. M. Morales, C. R. Landis and F. Weinhold, *NBO 6.0*, Theoretical Chemistry Institute, University of Wisconsin, Madison, WI, 2013, http://nbo6. chem.wisc.edu.

82 S. I. Gorelsky, *SWizard program*, http://www.sg-chem.net/, University of Ottawa, Ottawa, Canada, 2013.

83 S. I. Gorelsky and A. B. P. Lever, *J. Organomet. Chem.*, 2001, **635**, 187–196.

84 M. Cossi, V. Barone, R. Cammi and J. Tomasi, *Chem. Phys. Lett.*, 1996, **255**, 327–335.

85 V. Barone, M. Cossi and J. Tomasi, *J. Chem. Phys.*, 1997, **107**, 3210–3221.

86 F. Santoro, R. Improta, A. Lami, J. Bloino and V. Barone, *J. Chem. Phys.*, 2007, **126**, 084509.

87 F. Santoro, A. Lami, R. Improta and V. Barone, *J. Chem. Phys.*, 2007, **126**, 184102.

88 F. Santoro, A. Lami, R. Improta, J. Bloino and V. Barone, *J. Chem. Phys.*, 2008, **128**, 224311.

89 D. Licari, A. Baiardi, M. Biczysko, F. Egidi, C. Latouche and V. Barone, *J. Comput. Chem.*, 2015, **36**, 321–334.

90 T. Le Bahers, C. Adamo and I. Ciofini, *J. Chem. Theory Comput.*, 2011, **7**, 2498–2506.

91 I. Ciofini, T. Le Bahers, C. Adamo, F. Odobel and D. Jacquemin, *J. Phys. Chem. C*, 2012, **116**, 11946–11955.

92 D. Jacquemin, T. L. Bahers, C. Adamo and I. Ciofini, *Phys. Chem. Chem. Phys.*, 2012, **14**, 5383.